

Pulse-Width Modulation Neuron Implemented by Single Positive-Feedback Device

Sung Yun Woo, *Member, IEEE*, Dongseok Kwon, Byung-Gook Park, *Fellow, IEEE*, Jong-Ho Lee, *Fellow, IEEE* and Jong-Ho Bae, *Member, IEEE*

1 Abstract—Positive-feedback (PF) device and its operation scheme to implement pulse width modulation (PWM) function was proposed and demonstrated, and the device operation mechanism for implementing PWM function was analyzed. By adjusting the amount of the charge stored in the n floating body (Q_n), the potential of the floating body linearly changes with time. When Q_n reaches to a threshold value (Q_{th}), the PF device turns on abruptly. From the linear time-varying property of Q_n and the gate bias dependency of Q_{th} , fully functional PWM neuron properties including voltage to pulse width conversion and hard-sigmoid activation function were successfully obtained from a single PF device. A PWM neuron can be implemented by using a single PF device, thus it is beneficial to extremely reduce the area of a PWM neuron circuit than the previously reported one.

Index Terms—positive feedback, pulse width modulation, neuron device, hard-sigmoid activation function.

I. INTRODUCTION

As a result of recent interest in deep neural networks (DNNs), DNNs show similar level of inference performance to human for specific tasks, such as recognizing hand-written digits and classifying certain images [1]-[3]. However, the more complex the work required for DNN, the more complex the structure of the DNN and the more computations required. Hardware-based neural networks (HNNs) efficiently perform large-scale parallel multiply-accumulation (MAC) operations based on Ohm's and Kirchhoff's laws, and exponentially save power consumption compared to conventional computing systems [4]-[7]. There has been a lot of researches to utilize memory devices, such as resistive change memory (RRAM), phase change memory (PCRAM), and charge trap devices like FLASH [8]-[13], to represent synaptic weights and performing MAC operation. For MAC operation using the memory array, input data which is a set of raw data or the results of a MAC operation should be coded into a different form of signal by using a neuron circuit [14]. There are three mainstreams of the ways to input coding: pulse amplitude modulation (PAM), pulse width modulation (PWM), and pulse rate modulation (rate coding) [15]-[17]. PAM is simplest way for data coding, but it is inadequate for HNN because of the nonlinear output characteristics of most synaptic devices. Rate coding and PWM use voltage pulse with

constant amplitude, thus those are beneficial in terms of accurate MAC operation [18].

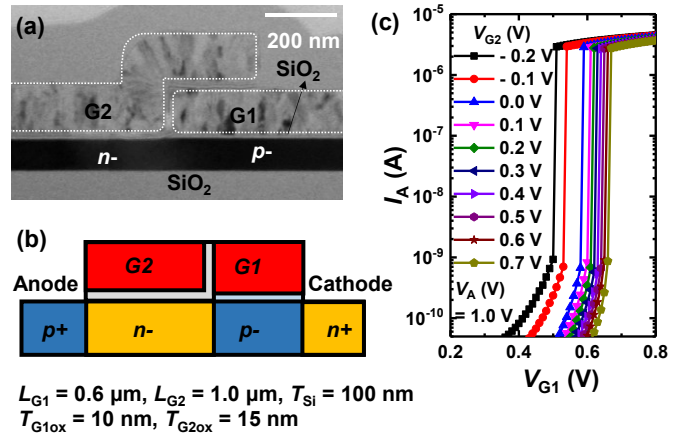


Fig. 1 (a) A TEM image and (b) a schematic cross-sectional view of the PF device. (c) The measured I_A - V_{G1} characteristics of the fabricated PF device at different V_{G2} , and V_A of 1 V.

Previously, we simulated an HNN using SPICE with a pulse-width modulation (PWM) neuron circuit consists of 13 transistors and one capacitor (13T-1C) [18]. It is noteworthy that the neuron circuit should be able to be integrated in a small area, considering that an HNN requires a very large number of neurons.

In this paper, a positive-feedback (PF) device and the novel operation scheme for implementing a PWM neuron is proposed. The PWM function was successfully demonstrated using a single PF device. Considering the size and the number of transistors for the previously reported PWM neuron circuit, the size of the PWM neuron can be extremely reduced with a single PF device. In addition, the voltage amplitude to pulse width conversion can be performed without capacitor in the PF device, thus the PWM neuron size would be reduced more.

II. DEVICE STRUCTURE AND POSITIVE FEEDBACK OPERATION

PF devices have been used to implement neuronal functions [19]-[22], thanks to their unique behavior. Fig. 1(a) and (b) show the cross-sectional schematic and SEM images of the PF device used in this work. The detailed fabrication step is described elsewhere [19]. The device has $p^+/n^-/p^-/n^+$ doped

This work was supported in part by the (ERC) and the National Research Foundation of Korea (NRF- 2016M3A7B4909604). The review of this letter was arranged by Editor XXX. (Corresponding authors: Jong-Ho Lee; Jong-Ho Bae.) S. Y. Woo, D. Kwon, B.-G. Park and J.-H. Lee are with the Department of Electrical and Computer Engineering and Inter-University Semiconductor

Research Center (ISRC), Seoul National University, Seoul 08826, Korea (e-mail: jhl@snu.ac.kr).

J.-H. Bae is with the School of Electrical Engineering, Kookmin University, Seoul 02707, Korea (e-mail: jbae@kookmin.ac.kr).

channel and two gates (G1 and G2) located next to each other on p^- - and n^- -doped region. The doping concentrations of n^-/p^- channel are 1×10^{18} and 3×10^{17} cm^{-3} , respectively. The lengths of G1 and G2 are $0.6 \mu\text{m}$ and $1.0 \mu\text{m}$, respectively, and the thickness of $p^+/n^-/p^-/n^+$ doped channel is 100 nm . Gate insulator for G1 is SiO_2 with thickness of 10 nm and for G2 has EOT of 15 nm . This PF device is basically two connected floating body MOSFETs: n^- - and p^- -MOSFET having G1 and G2 as a gate, respectively. These MOSFETs are

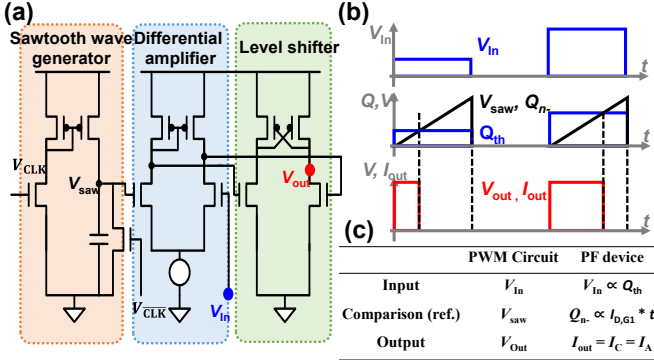


Fig. 2 (a) A schematic diagram of a PWM circuit [F1] (reproduced from [F1] with permission). (b) Schematic diagram of elements for implementing PWM function. (c) The functional element of a PF device for implementing PWM function.

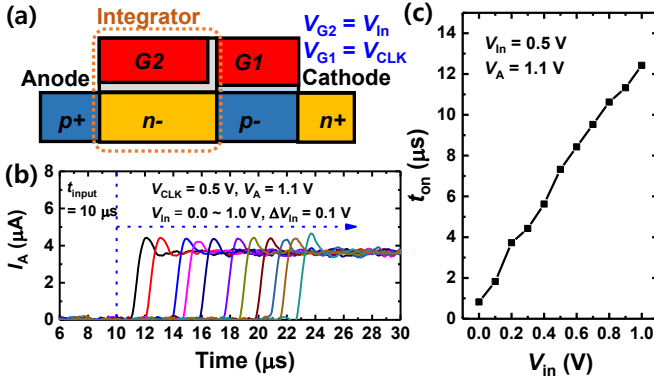


Fig. 3 (a) A bias scheme for measuring the PF device. (b) The measured transient responses ($t-I_A$) of the PF device under different V_{in} and (c) the relationship between V_{in} and t_{on} .

connected in series and their drains are respectively connected to the bodies of each other. When both the MOSFETs are turned-off, applying a positive anode bias ($V_A > 0$) with grounded cathode ($V_C = 0$) cannot turn on the device due to the reverse-biased $p-n$ diode formed by n^-/p^- junction. However, when a positive G1 bias (V_{G1}) is applied, which is a gate bias of n^- -MOSFET, electrons are injected from the cathode to the n^- region and stored, which is the drain of the n^- -MOSFET and the body of the p^- -MOSFET. In that case, the threshold voltage of p^- -MOSFET (V_{Tp}) increases due to the floating body effect. As V_{Tp} increases, the amount of the hole injection from anode to p^- region exponentially increases and it also reduces the threshold voltage of n^- -MOSFET (V_{Tn}), therefore, more holes are injected from the anode to the p^- region. In summary, the drain current of n^- -MOSFET (I_{Dn}) injects electron and the stored electron in n^- floating body (Q_n) change V_{Tp} to increase I_{Dp} , thus p^- -

MOSFET turns on and a positive feedback loop is formed. When $|Q_n|$ is larger than a threshold value (Q_{th}), the device is turned on and operates as a diode. Fig. 1(c) shows the anode current (I_A) versus V_{G1} as a function of G2 bias (V_{G2}). Due to the positive-feedback operation, I_A changes abruptly as V_{G1} changes. It is worth noting that the turn-on V_{G1} ($V_{G1,on}$) increases as V_{G2} increases. As V_{G2} increases, V_{Tp} should be larger to turn-on the PF device, which means larger Q_{th} is required.

III. PULSE-WIDTH-MODULATION (PWM) OPERATION

The previously proposed PWM circuit consists of three functional circuit elements, a sawtooth wave generator, a differential amplifier and a level shifter (see Fig. 2(a)). The two inputs of

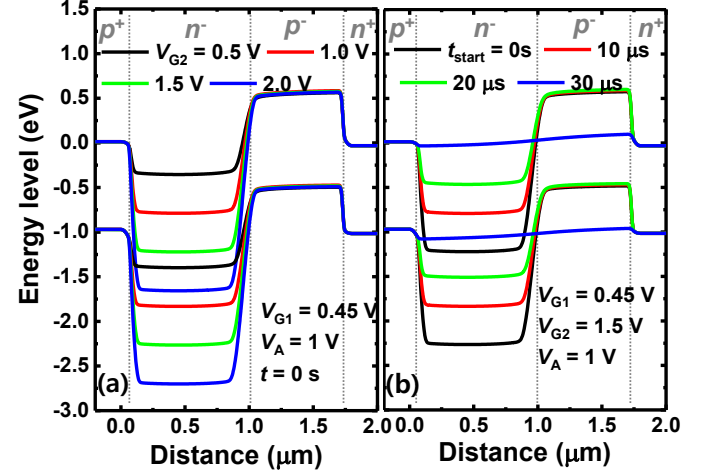


Fig. 4 (a) Energy band diagrams of a PF device along the silicon channel at different V_{G2s} ($=V_{in}$ s). (b) Energy band diagrams of a PF device along the silicon channel over time, at $V_{G1} = 0.45 \text{ V}$, $V_{G2} = 1.5 \text{ V}$ and $V_A = 1 \text{ V}$.

the differential amplifier are the input data coded in a constant voltage amplitude (V_{in}) and a triangular voltage pulse train ($V_{saw}(t)$) generated by the sawtooth wave generator. In the sawtooth wave generator, a signal of $V_{saw}(t) = I/C_{saw}(t - t_0)$ is generated when clock (CLK) is 1, where t_0 is the time when CLK becomes 1 and the voltage increasing rate is the ratio between the pull-up current of the p^- -MOSFET (I) and the capacitance (C_{saw}). As shown in Fig. 2(b), if $V_{in} > V_{saw}(t)$, the result of the differential amplifier (V_{Diff}) is 1 and if not, V_{Diff} is 0. Considering $V_{saw}(t)$ is linear function of the time, the time for $V_{in} > V_{saw}(t)$ and the pulse width (t_p) of V_{diff} are linearly proportional to V_{in} . Note that $V_{saw} = V_{DD}$ and $V_{saw}(t) > V_{in}$ when CLK is 0, thus maximum t_p (t_{max}) is $1/f_{CLK}$ where f_{CLK} is the clock frequency. Therefore, V_{in} is linearly converted to a V_{Diff} pulse with t_p in the range of $[0, t_{max}]$. V_{Diff} pulse is shifted to a desired voltage level in the level shifter as an output voltage pulse (V_{out}), and is used as a signal for the next layer. To summarize, the basic principle to implement PWM function is comparing a input signal (V_{in}) and a signal ($V_{saw}(t)$) that varies linearly with time during a clock cycle. Those can be realized by a single PF device as described in Fig. 2(b) and (c), which will be discussed in the following.

IV. IMPLEMENTATION OF PWM FUNCTION USING A SINGLE PF DEVICE

The PWM function was implemented from a fabricated PF device by applying V_{G1} and V_{G2} as a CLK bias (V_{CLK}) and V_{in} , respectively, as shown in Fig. 3. As $V_{G2} = V_{in}$ increases, the time to turn-on the PF device (t_{on}) increases (Fig. 3(b)), and V_{in} and t_{on} has a linear relationship (Fig. 3(c)). This result implies that the fabricated PF device can operate as a linear V_{in} - t_p converter in a certain range.

In order to analyze the origin of the linear relationship between V_{in} and t_{on} which is a key mechanism of implementing PWM function, a simulation study was conducted with a TCAD simulator (Sentaurus) of Synopsys (Figs. 4 and 5). As $V_{G2} = V_{in}$ increase, the energy band at n region linearly moves down and V_{Tp} linearly decreases (Fig. 4(a)), because the n region is floated and is deep-depleted. The key is that the degree of deep-depletion is linearly proportional to the $V_{G2} = V_{in}$, and Q_{th} linearly increases. Considering $V_{G1} = V_{CLK} = 0.45$ V and assuming the source of Q_n is I_{Dn} , $|Q_n|$ increases linearly proportional to the time and $|Q_n| = I_{Dn}(t - t_0)$. Thus, the energy band at n region moves upward as time goes by, as shown in Fig. 4(b). In terms of implementing PWM function, $Q_{th}(V_{in})$ at $t = t_0$ is the constant input signal and $|Q_n(t)|$ is the linear time-varying signal (see Fig. 2(b) and (c)). These two signals are compared whether $Q_{th}(V_{in}) > |Q_n(t)|$ or not. When $Q_{th}(V_{in}) > |Q_n(t)|$, p -MOSFET does not turn-on. When $Q_{th}(V_{in}) < |Q_n(t)|$, p -MOSFET turns on and the PF device turns on due to the positive feedback operation, as explained in Section II.

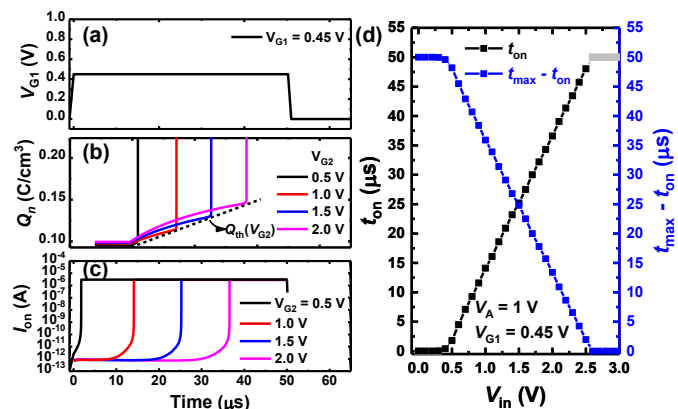


Fig. 5 (a) V_{CLK} , (b) Q_n and (c) I_n over time at various $V_{G2} (=V_{in})$. (d) $V_{in} - t_{on}$ (left y-axis) and $V_{in} - (t_{max} - t_{on})$ (right y-axis) plots which indicates activation function of the proposed PWM function implemented by a PF device.

Fig. 5(b) shows $|Q_n(t)|$ where $V_{G2} = V_{in}$ varies from 0.5 V to 2.0 V, when $V_{G1} = V_{CLK} = 0.45$ V (see Fig. 5(a)). As $V_{G2} = V_{in}$ increases, Q_{th} and t_{on} linearly increases, as shown in Fig. 5(b) and (c). Therefore, a linear relationship between $V_{G2} = V_{in}$ and t_{on} is obtained. PF device is off ($I_n \sim 1$ pA) when $V_{CLK} = 0$, thus t_{max} is $1/f_{CLK}$. This result indicates V_{in} is successfully converted to t_{on} with linear relationship in the range of $[0, t_{max}]$, and the pulse width is $t_{max} - t_{on}$. The relationship between V_{in} and t_{on} is the hard-sigmoid activation function between 0 and t_{max} , and it can be modulated by using additional circuitry, such as a simple

inverter. Therefore, the proposed PF device with this operation scheme is a PWM neuron that effectively implements both a V_{in} to t_p converter and a hard-sigmoid activation function.

V. CONCLUSION

PWM function is implemented by using a single PF device with two gates. V_{G1} is V_{CLK} which is linearly increase $|Q_n|$ when $CLK = 1$, and V_{Tp} linearly increases as time goes by. By applying input signal to V_{G2} , Q_{th} is linearly changed and comparison between $|Q_n|$ and Q_{th} is performed, and the result is amplified by the positive feedback operation. The proposed positive feedback device effectively integrates the two basic function elements of PWM circuits: generating linear time-varying variable ($|Q_n|$) and comparing it with input signal (Q_{th}). Therefore, the PWM circuit including a capacitor can be replaced by a single positive feedback, which is beneficial to integrate neuron circuits for neural network area.

REFERENCES

- [1] S. Yu, "Neuro-inspired computing with emerging nonvolatile memories," *Proc. IEEE*, vol. 106, no. 2, pp. 260–285, Feb. 2018, doi: 10.1109/jproc.2018.2790840.
- [2] R. Andri, L. Cavigelli, D. Rossi and L. Benini, "YodaNN: An Architecture for Ultralow Power Binary-Weight CNN Acceleration," *IEEE Transactions on Computer-Aided Design of Integrated Circuits and Systems*, vol. 37, no. 1, pp. 48–60, Jan. 2018, doi: 10.1109/TCAD.2017.2682138.
- [3] L. Gao, P. Chen and S. Yu, "Demonstration of Convolution Kernel Operation on Resistive Cross-Point Array," *IEEE Electron Device Letters*, vol. 37, no. 7, pp. 870–873, July 2016, doi: 10.1109/LED.2016.2573140.
- [4] F. Su, W.-H. Chen, L. Xia, C.-P. Lo, T. Tang, Z. Wang, K.-H. Hsu, M. Cheng, J.-Y. Li, Y. Xie, Y. Wang, M.-F. Chang, H. Yang, and Y. Liu, "A 462GOPS/J RRAM-based nonvolatile intelligent processor for energy harvesting IoE system featuring nonvolatile logics and processing-in-memory," *Symposium on VLSI Technology*, 2017, pp. T260–T261, doi: 10.23919/VLSIT.2017.7998149.
- [5] A. Shafiee, A. Nag, N. Muralimanohar, R. Balasubramanian, J. P. Strachan, M. Hu, R. S. Williams, and V. Srikumar, "ISAAC: A convolutional neural network accelerator with in-situ analog arithmetic in crossbars," *ACM/IEEE 43rd Annu. Int. Symp. Comput. Archit. (ISCA)*, 2016, doi: 10.1109/isca.2016.12.
- [6] S. Yu, Z. Li, P.-Y. Chen, H. Wu, B. Gao, D. Wang, W. Wu, and H. Qian, "Binary neural network with 16 Mb RRAM macro chip for classification and online training," *Proc. IEEE Int. Electron Devices Meeting (IEDM)*, 2016, pp. 16.2.1–16.2.4, doi: 10.1109/IEDM.2016.7838429.
- [7] M. Hu, J. P. Strachan, Z. Li, E. M. Grafals, N. Davila, C. Graves, S. Lam, N. Ge, J. J. Yang, and R. S. Williams, "Dot-product engine for neuromorphic computing: Programming 1T1M crossbar to accelerate matrix-vector multiplication," *Proc. 53rd Annu. Design Autom. Conf. (DAC)*, 2016, doi: 10.1145/2897937.2898010.
- [8] S. Y. Woo, K.-B. Choi, S. Lim, S.-T. Lee, C.-H. Kim, W.-M. Kang, D. Kwon, J.-H. Bae, B.-G. Park, J.-H. Lee, "Synaptic device using a floating fin-body MOSFET with memory functionality for neural network," *Solid-State Electronics*, vol. 156, pp.23–27, June 2019, doi: 10.1016/j.sse.2019.02.011
- [9] S. Lee, H. Kim, J.-H. Bae, H. Yoo, N. Y. Choi, D. Kwon, S. Lim, B.-G. Park, and J.-H. Lee "High-Density and Highly-Reliable Binary Neural Networks Using NAND Flash Memory Cells as Synaptic Devices," *2019 IEEE International Electron Devices Meeting (IEDM)*, 2019, pp. 38.4.1–38.4.4, doi: 10.1109/IEDM19573.2019.8993478.
- [10] Q. Zhang, H. Wu, P. Yao, W. Zhang, B. Gao, N. Deng, H. Qian, "Sign backpropagation: An on-chip learning algorithm for analog RRAM neuromorphic computing systems," *Neural Netw.*, vol. 108, pp. 217–223, Dec. 2018, doi: 10.1016/j.neunet.2018.08.012.
- [11] M. Prezioso, Y. Zhong, D. Gavrillov, F. Merrikh-Bayat, B. Hoskins, G. Adam, K. Likharev, and D. Strukov, "Spiking neuromorphic networks with metal-oxide memristors," *Proc. IEEE Int. Symp. Circuits Syst. (ISCAS)*, May 2016, pp. 177–180, doi: 10.1109/ISCAS.2016.7527199.

- [12] S. Sidler, A. Pantazi, S. Woźniak, Y. Leblebici, and E. Eleftheriou, "Unsupervised learning using phase-change synapses and complementary patterns," in *Proc. Artif. Neural Netw. Mach. Learn. (ICANN)*, in Lecture Notes in Computer Science, vol. 10613. Cham, Switzerland: Springer, 2017, 2017, doi: 10.1007/978-3-319-68600-4_33.
- [13] W. Kim, R.L. Bruce, T. Masuda, G.W. Fraczak, N. Gong, P. Adusumilli, S. Ambrogio, H. Tsai, J. Bruley, J.-P. Han, M. Longstreet, F. Carta, K. Suu and M. BrightSky, "Confined PCM-based Analog Synaptic Devices offering Low Resistance-drift and 1000 Programmable States for Deep Learning," *2019 Symposium on VLSI Technology*, 2019, pp. T66-T67, doi: 10.23919/VLSIT.2019.8776551.
- [14] S. Lim, J.-H. Bae, J.-H. Eum, S. Lee, C.-H. Kim, D. Kwon, B.-G. Park, and J.-H. Lee, "Adaptive learning rule for hardware-based deep neural networks using electronic synapse devices," *Neural Comput. Appl.*, vol. 31, pp. 8101–8116, Jul. 2018, doi: 10.1007/s00521-018-3659-y.
- [15] T. Kim, H. Kim, J. Kim and J. Kim, "Input Voltage Mapping Optimized for Resistive Memory-Based Deep Neural Network Hardware," *IEEE Electron Device Letters*, vol. 38, no. 9, pp. 1228-1231, Sept. 2017, doi: 10.1109/LED.2017.2730959.
- [16] N. Qiao, H. Mostafa, F. Corradi, M. Osswald, F. Stefanini, D. Sumislawska, and G. Indiveri, "A reconfigurable on-line learning spiking neuromorphic processor comprising 256 neurons and 128K synapses." *Frontiers Neuroscience*, vol. 9, article 141, pp.1-17, Apr. 2018, doi: 10.3389/fnins.2015.00141.
- [17] S. Lim, J.-H. Bae, J.-H. Eum, S. Lee, C.-H. Kim, D. Kwon, and J.-H. Lee, "Hardware-based Neural Networks using a Gated Schottky Diode as a Synapse Device," *Proc. IEEE Int. Symp. Circuits Syst. (ISCAS)*, 2018, pp. 1-5, doi: 10.1109/ISCAS.2018.8351152.
- [18] S. Lim, D. Kwon, J.-H. Eum, S.-T. Lee, J.-H. Bae, H. Kim, C.-H. Kim, B.-G. Park, and J.-H. Lee, "Highly Reliable Inference System of Neural Networks Using Gated Schottky Diodes," *IEEE J. Electron Devices Soc.*, vol. 7, pp. 522-528, April 2019, doi: 10.1109/JEDS.2019.2913146.
- [19] S. Y. Woo, D. Kwon, N. Choi, W.-M. Kang, Y.-T. Seo, M.-K. Park, J.-H. Bae, and B.-G. Park, and J.-H. Lee, "Low-Power and High-Density Neuron Device for Simultaneous Processing of Excitatory and Inhibitory Signals in Neuromorphic Systems," *IEEE Access*, vol. 8, pp. 202639-202647, 2020, doi: 10.1109/ACCESS.2020.3036088.
- [20] M. Kwon, K. Park, M. Baek, J. Lee and B. Park, "A Low-Energy High-Density Capacitor-Less I&F Neuron Circuit Using Feedback FET Co-Integrated With CMOS," *IEEE J. Electron Devices Soc.*, vol. 7, pp. 1080-1084, Sep. 2019, doi: 10.1109/JEDS.2019.2941917.
- [21] K.-B. Choi, S. Y. Woo, W.-M. Kang, S. Lee, C.-H. Kim, J.-H. Bae, S. Lim and J.-H. Lee, "A Split-Gate Positive Feedback Device with an Integrate-and-Fire Capability for a High-Density Low-Power Neuron Circuit," *Frontiers in Neuroscience*, vol. 12, pp. 1-13, Oct. 2018, doi: 10.3389/fnins.2018.00704.
- [22] Min-Woo Kwon, Myung-Hyun Baek, Sungmin Hwang, Kyungchul Park, Tejin Jang, Taehyung Kim, Junil Lee, Seongjae Cho, and Byung-Gook Park, "Integrate-and-fire neuron circuit using positive feedback field effect transistor for low power operation," *Journal of applied physics*, vol. 124, pp. 152107, Sep. 2018, doi: 10.1063/1.5031929